MAGNETIC FIELDS AND THE STRUCTURE OF THE SOLAR CORONA

II: *Observations of the 12 November 1966 Solar Corona*

GORDON NEWKIRK, JR. and ROBERT G. DUPREE
High Altitude Observatory, National Center for Atmospheric Research, Boulder, Colo., U.S.A.*

and

EDWARD J. SCHMAHL
University of Colorado, Dept. of Astro-Geophysics, Boulder, Colo., U.S.A.

(Received 17 June, 1970)

Abstract. During the eclipse of 12 November 1966, the solar corona was photographed at an effective wavelength of 6500 Å with an *f*/16, 11.1 cm aperture camera. Reduction of the observations yields coronal radiances and polarizations from 1.4 to 3.5 solar radii. Standard techniques are used for the separation of *F* and *K*-coronas, determination of coronal electron densities and temperatures, and estimation of the orientation of the major streamers in space.

1. Equipment

The data used in this analysis were photographic observations of the solar corona made during the eclipse of 12 November, 1966 (13^h26^m UT) from Pulacayo, Bolivia (altitude 3.4 km). Table I contains a summary of the technical characteristics of the camera while Table II lists the photographs obtained. All images were calibrated photometrically by the impression of a step wedge at the side of each frame while the

TABLE I

Characteristics of the coronal camera

Objective:	Goertz triplet, 11.1 cm effective aperture, 178 cm focal length
Field:	3.°1 (5.8 $D_\odot$) diameter on diagonal
Plate scale:	115.8 sec of arc per mm
Resolution	0.7 sec of arc (diffraction limit)
at 6500 Å:	1.3 sec of arc (measured, objective alone)
	3 sec of arc (measured, objective-film combination)
Film:	70 mm, Kodak Shellburst, developed Kodak D-70 (1:1) 8^m nitrogen burst agitation (1^s burst, 15^s interval)
Wavelength:	6500 Å effective wavelength – Band pass about 1400 Å
Filters:	Radially graded, metal on glass (Optical Coating Lab., Inc.)
	Three, HN-38 polaroidfilters with anti-reflection coating oriented at 60° intervals.
	Wratten 25 Å filters sandwiched on each of above. All located at focal plane.
Micro-photometer:	Slit 4.6 sec arc × 38.2 sec arc

* The National Center for Atmospheric Research is sponsored by the National Science Foundation.

Solar Physics **15** (1970) 15–39.

TABLE II

Sequence of eclipse photographs

Number	Filter used	Exposure time
1	Radially graded	1s
2	Radially graded	10s
3	Polaroid 1 (*E* vector 60°E, geocentric)	1s
4	Polaroid 1 (*E* vector 60°E, geocentric)	10s
5	Polaroid 2 (*E* vector north, geocentric)	1s
6	Polaroid 2 (*E* vector north, geocentric)	10s
7	Polaroid 3 (*E* vector 60°W, geocentric)	1s
8	Polaroid 3 (*E* vector 60°W, geocentric)	10s
9	Clear	0.13s
10	Clear	1.5s
11	Clear	15s

current and voltage drawn by the illuminating lamp were controlled during the observing period. In order to photograph the entire corona with a single exposure, two frames were made through a radially graded, neutral filter whose transmission function (Figure 1) was chosen to compensate for the steep decrease of coronal radiance with distance above the photosphere. We did not employ either of these photographs (Figure 2) for quantitative analysis. Guiding accuracy during totality was to within 0.05 sec arc per second of time of the solar rate in right ascension with a declination drift of approximately 0.02 sec arc per second of time. Visual estimates of the seeing

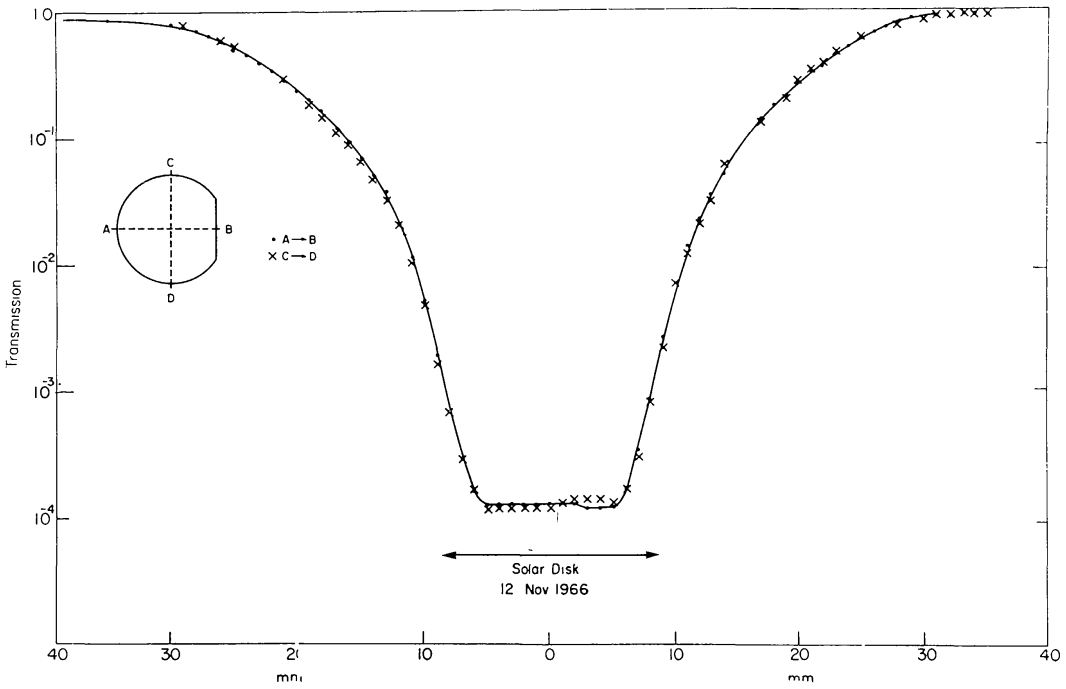

Fig. 1. Transmission function of the radially graded, neutral filter used to produce the photograph of the corona shown in Figure 2.

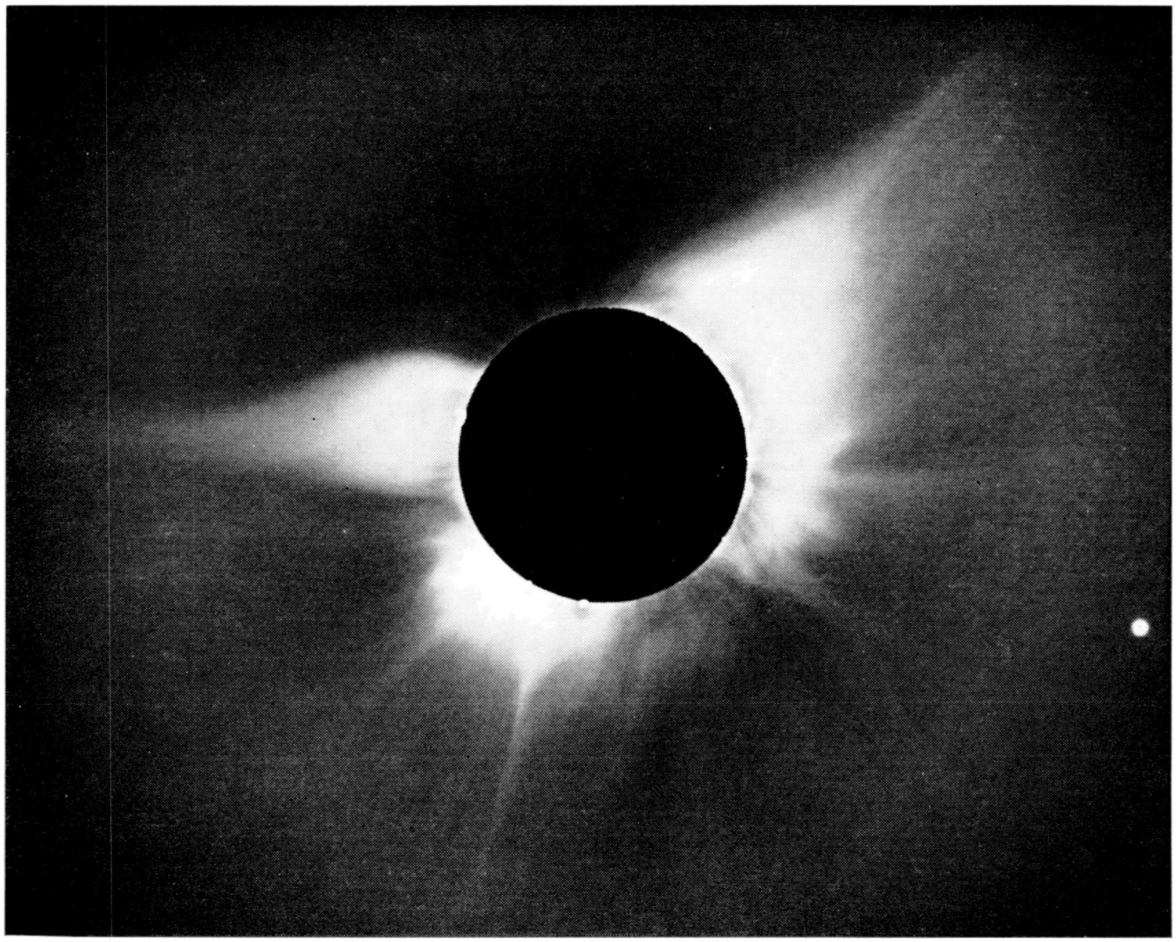

Fig. 2. The solar corona of 12 November, 1966 photographed through the radially graded, focal plane filter of Figure 1 with an exposure of 10^s. The over-exposed image of Venus appears in the North-east quadrant at position angle 72° (geocentric).

during totality suggest that the resolution of the final photographs is about 6 sec arc rather than the 3 sec arc of which the system is capable.

2. Determination of Positions in the Corona

Accurate polarimetry requires that microdensitometer measurements be made at the same locations in the corona on a number of separate photographs. The obvious method of establishing a coordinate system from measurements of the moon's limb and the known orientation of the camera could be applied to only the three weakest exposures (the two made with the radially graded filter and the 0.13 second, clear). Halation of light from the inner corona prevented determination of the lunar limb on the remaining exposures. Rather than use the weaker exposures to establish a basic coordinate system to be transferred to the others by measurement of fiducial marks on the film, we used the image of Venus and the presence of several fine scratches along the entire length of the film as references. Measurement of the orientation of the scratches on the weaker exposures showed that these lines established a reference direction with frame to frame deviations of less than $\pm 0.1°$. All sources considered,

the error in locating a given position in the corona from one plate to another was less than $\pm 50\ \mu$ (5.8 sec arc). Repeated 'identical' radial scans of the same plate, with the plate's being removed and realigned between scans, were found to be identical to within 0.5% in coronal radiance.

3. Photometry

The impression of a standard wedge of carefully controlled radiance on each photograph establishes only a relative photometric scale. This scale was related to the *mean radiance of the solar disk* $B_\odot$ by exposures made the day before the eclipse around 13^h30^m UT with six secondary standard opals ranging in radiance from $8.0\times10^{-7}\ B_\odot$ to $7.0\times10^{-10}\ B_\odot$ placed over the entire objective lens. Exposures of the disk of the sun with a 0.318 cm diameter diaphragm and neutral filter over the objective just before the above calibration sequence as well as 20^m after totality served as an additional check of the constancy of the radiance of the standard wedge. The radiances of the full aperture standard opals were determined by photoelectric comparison with a set of primary opals which have been calibrated geometrically.

Because the standard lamp could not be operated as its designed power, those portions of the corona brighter than $B/B_\odot = 1.6\times10^{-7}$ ($r \leqslant 1.4\ R$) are poorly measured. For $1.4\ R \leqslant r \leqslant 3.5\ R$ the internal consistency of the data suggests that relative radiances are accurate to $\pm 5\%$. As can be seen from the development below, these uncertainties imply standard deviations in any of the Stokes parameters of about $\pm 7\%$, in the polarization of $\pm 8.6\%$, and in the polarization angle of $\pm 10°$. Although estimates of the absolute accuracy of such data are uncertain, we believe these data yield the coronal radiance at 6500 Å to an accuracy of $\pm 10\%$.

Since both the Stokes representation and the usual 'practical' polarization parameters have advantages for describing the corona, we have reduced our measures in both systems. All data were corrected for the fact that real rather than perfect polarizers were used in the observation. If B is the coronal radiance measured through a perfect polarizer and B' is that measured through a real polarizer, whose principal transmissions are k_1 and k_2 (Shurcliff, 1962), the ratio of these two radiances will be

$$\frac{B'}{B} = \frac{(k_1 + k_2)\, I + (k_1 - k_2)\, Q \cos 2\alpha}{I + Q \cos 2\alpha}, \tag{1}$$

where I and Q are the usual Stokes parameters and α is the angle between the k_1 axis and the E vector of the radiation. When $k_1 \gg k_2$ Equation (1) reduces to

$$B'/B \sim k_1 .$$

Laboratory measurement showed the polaroid orientations of our system to be within $\pm 0.^\circ 8$ of those listed in Table II while the transmissions of parallel and crossed polaroids implied principal transmissions k_1 and k_2 and transmission to unpolarized light t listed in Table III. These quantities were used in the approximate form of Equation (1) for the radiances B_1, B_2 and B_3 as seen through perfect polaroids oriented as in Table II.

TABLE III

Polaroid transmissions

Polaroid number	k_1	k_2	t
1	0.834	0.00058	0.417
2	0.934	0.00044	0.467
3	0.855	0.00061	0.427

The Stokes parameters for any point in the corona are then

$$\left.\begin{aligned} I &= \tfrac{2}{3}(B_1 + B_2 + B_3), \\ Q &= \tfrac{2}{3}(2B_1 - B_2 - B_3), \\ U &= \tfrac{2}{3}\sqrt{3}(B_3 - B_2), \\ V &= 0. \end{aligned}\right\} \quad (2)$$

Each of the quantities refers to the total radiance contributed by the *K*-corona, *F*-corona, instrumental scattering, and the sky in *units of the mean solar disk at* 6500 Å with the convention of the observer looking into the arriving beam. The usual parameters of radiance I, polarization p, and polarization angle are

$$\begin{aligned} I &= I, \\ p &= \sqrt{Q^2 + U^2}, \\ \psi &= \tfrac{1}{2}\arctan(U/Q), \end{aligned} \quad (3)$$

where ψ is the angle between the H vector and position angle 330° (geocentric) counting east.

4. Instrumental and Sky Contributions

The raw measures of radiance must be corrected for the presence of the spurious contributions of the instrument and the sky. In making these corrections we have borne in mind that only the observations at $r > 1.4\ R$ are accurate and that correction to the lower coronal data would be futile. Moreover, we must acknowledge that the instrumental and sky contributions, A and S respectively, are for all practical purposes inseparable since an independent measure of one or the other was not made.

The simplest evaluation of contribution I_{A+S} is that of the radiance of the lunar disk. However, this radiance was so low that the measures fall on the toe of the characteristic curve of the photographic emulsion. Thus, no great confidence can be placed on the value

$$I_{A+S} = 2.06 \pm 0.4 \times 10^{-9} B_\odot$$

obtained in that manner.

We also estimated the radiance I_{A+S} by reference to the radiance and radial decrease of the *F*- and *K*-coronas determined previously by other authors. Assume that the equatorial *F*- and *K*-coronas of 12 November, 1966 differed from those

observed in 1963 (Gillett *et al.*, 1964; Blackwell and Petford, 1966) only by constant factors. Thus, the total radiance I for the equatorial scans is

$$I = C_1 K_{1963} + C_2 F_{1963} + I_{A+S}, \tag{4}$$

where the Gillett *et al.* data were used in the inner corona and the Blackwell and Petford data were used in the outer corona. The least squares fit of (4) yields

$$C_1 = 1.13 \pm 0.77$$

$$C_2 = 0.63 \pm 0.32$$

$$I_{A+S} = 1.48 \pm 0.19 \times 10^{-9} B_\odot .$$

Clearly, the large errors in the coefficients C_1 and C_2 reflect the variation of the K-corona among the eight equatorial scans and the uncertainty caused by the fact that the K and F contributions represent nearly parallel functions. I_{A+S} is more satisfactorily determined.

The polarization of the sky and instrumental contributions may be evaluated by taking account of the fact that the sum of the K and F-coronas is polarized with E vector tangent to the solar limb (Ney *et al.*, 1961). Thus, two independent parameters (I and p) completely describe the corona and the three Stokes parameters I,

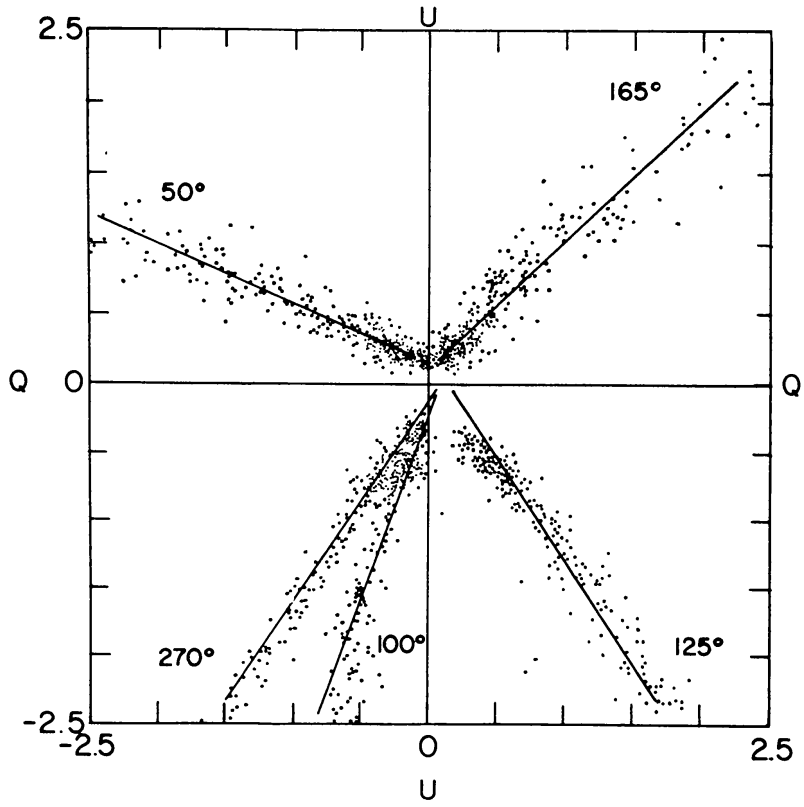

Fig. 3. The Stokes parameters Q and U for radial scans at position angles 50°, 100°, 125°, 165° and 270°. The straight lines indicate the dependence calculated for $Q_{A+S} = 0.04 \times 10^{-9} B_\odot$, $U_{A+S} = = 0.01 \times 10^{-9} B_\odot$ and a tangentially polarized $F+K$-corona. Lines from all other scans pass within 0.15×10^{-9} of this point.

Q, and U derived from three symmetrically oriented polaroids must be linearly related. This may be more clearly seen from the relations

$$\begin{aligned} U &= Ip \sin 2\psi = (Ip)_{K+F} \sin 2\psi_{K+F} + (Ip)_{A+S} \sin 2\psi_{A+S}, \\ Q &= Ip \cos 2\psi = (Ip)_{K+F} \cos 2\psi_{K+F} + (Ip)_{A+S} \cos 2\psi_{A+S}. \end{aligned} \tag{5}$$

Since ψ_{K+F} = constant along a radius in the corona and we assume, as a first approximation, that $(Ip)_{A+S}$ and ψ_{A+S} are constant over the entire field of view, a plot of U vs Q along a given radius should yield a straight line. Moreover, the lines of U vs Q for a variety of position angles should all intersect at the point Q_{A+S}, U_{A+S}. Figure 3 demonstrates that these inferences are, indeed, true. The intersection of the least squares lines fitted to the U vs Q plots for the thirty-eight radial scans used in this analysis yields

$$\begin{aligned} Q_{A+S} &= 0.04 \pm 0.02 \times 10^{-9} B_{\odot}, \\ U_{A+S} &= 0.01 \pm 0.01 \times 10^{-9} B_{\odot}. \end{aligned}$$

Since these values are much smaller than radiances in the outer corona, we ignore the instrumental and sky polarization in the final reduction.

The fact that the U vs Q plots for radial scans are linear strongly suggests that no

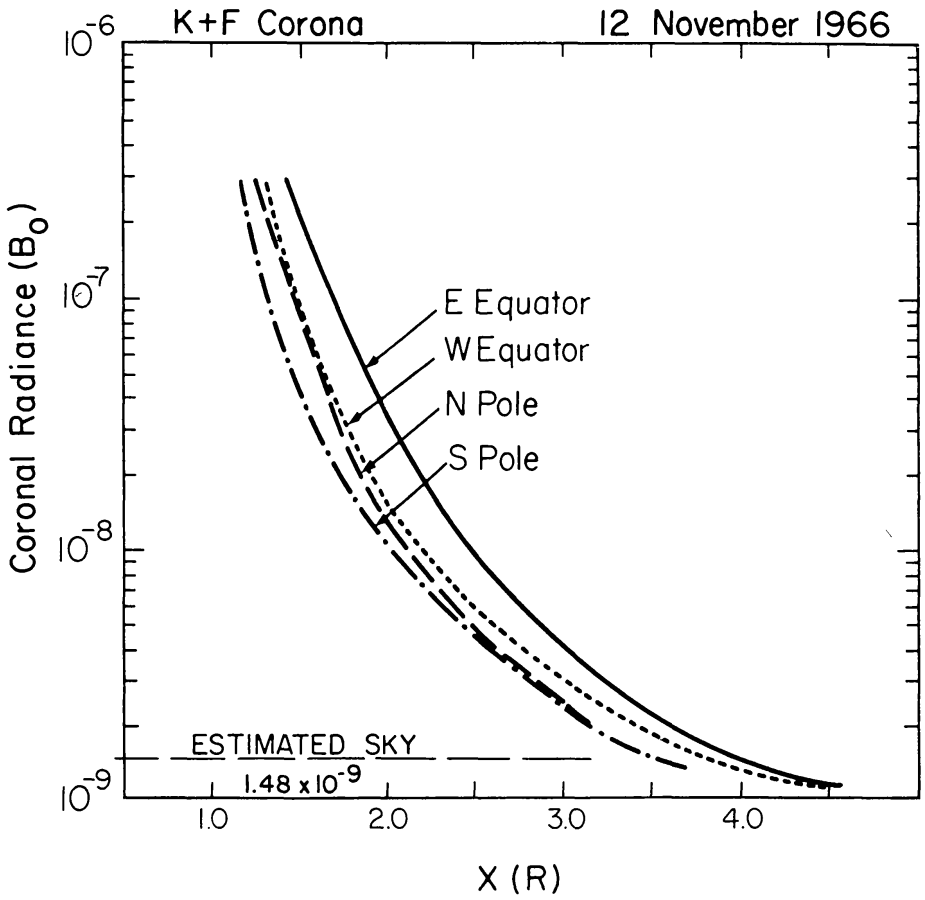

Fig. 4. The radiance of the $K+F$-corona for equatorial and polar scans. The observations have been corrected for the radiance of the sky.

positionally dependent aureole of instrumentally scattered or sky radiation contaminates the observations. This presumption is also borne out by measures on the lunar disk which yield

$$Q_{A+S} = -0.26 \pm 0.10 \times 10^{-9} B_{\odot},$$
$$U_{A+S} = -0.06 \pm 0.09 \times 10^{-9} B_{\odot}.$$

Although these values are, indeed, larger than those inferred above, they refer to light scattered at angles less than 0.5 R from the intense inner corona and, thus, can be safely ignored as a correction for the outer corona.

We summarize the contribution of the sky during totality employed during subsequent analysis as:

$$I_{A+S} = 1.48 \pm 0.19 \times 10^{-9} B_{\odot},$$
$$p_{A+S} = 0.03 \pm 0.02,$$
$$\psi_{A+S} = 7^{\circ} \pm 10^{\circ} (E \text{ vector} \sim \text{vertical}).$$

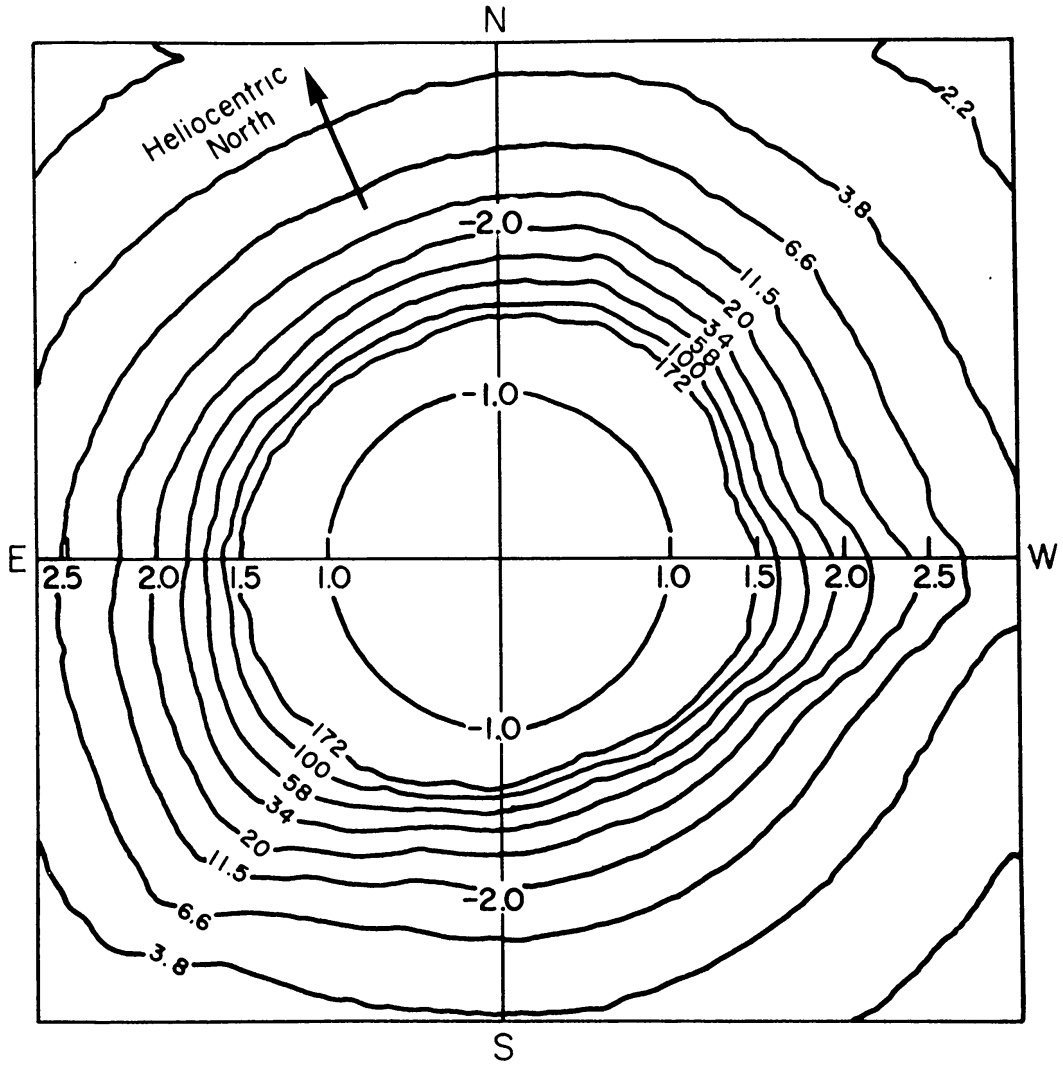

Fig. 5. Isophotes of the $K+F$-corona of 12 November, 1966 in units of $10^{-9} B_{\odot}$. The interval between adjacent isophotes is a factor of 1.72. Coordinates are geocentric.

5. Summary and Comparison with Other Observations

The present observations are summarized graphically in Figures 4–8. Figure 4 contains the radiance of the $F+K$-coronas for equatorial and polar scans after correction for the inferred sky contribution. In Figure 5 appear isophotes of the $F+K$-coronas in units of $10^{-9}\ B_{\odot}$ while in Figure 6 appear isopleths of the polarization. Again in both cases the data have been corrected for the sky. The orientation of the E-vector (Figure 7) confirms, to within the standard deviation of 0°.7, the observation of Ney *et al.* (1961) that the plane of polarization of the $F+K$-coronas is tangent to the limb.

A comparison between the measurements of the $F+K$-coronas summarized in Figure 5 with those made by Waldmeier (1967) and by Saito (private communication) as well as with the quantity pI determined by the HAO K-coronameter (Hansen *et al.*, 1967) reveals some differences in the scales of radiance. Closer analysis shows that

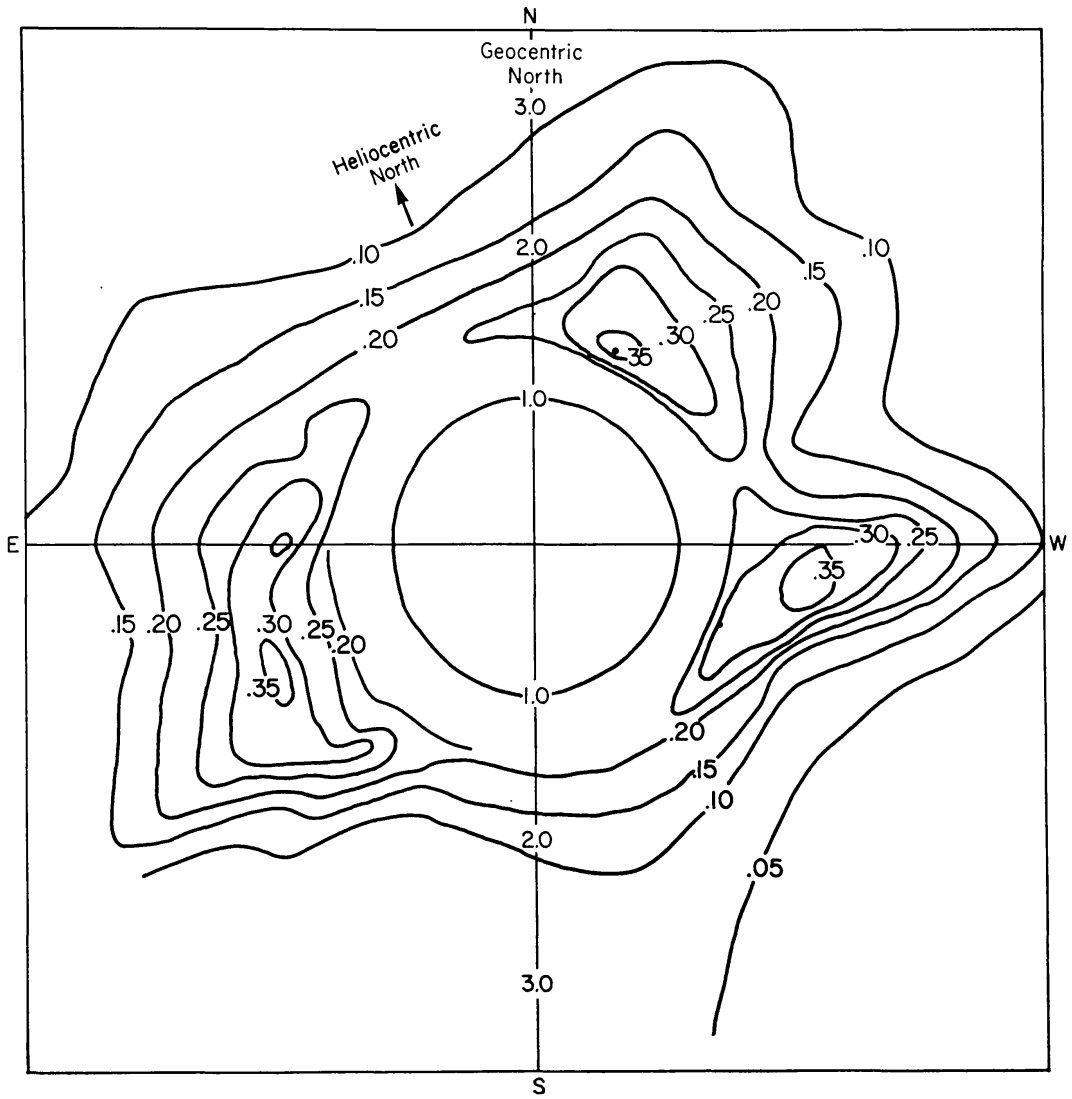

Fig. 6. Isopleths of polarization of the $F+K$-corona of 12 November, 1966 under the assumption that $I_{A+S} = 1.48 \times 10^{-9}$. Coordinates are geocentric.

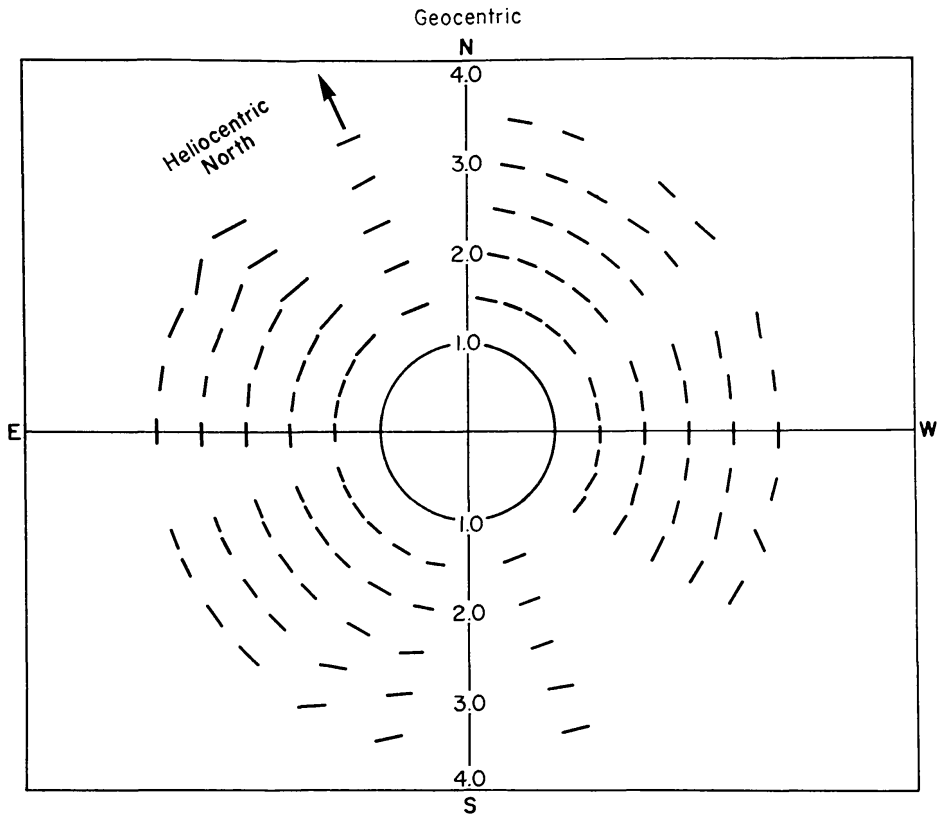

Fig. 7. Orientation of the electric vector in the $K+F$-corona of 12 November, 1966. Coordinates are geocentric.

the differences cannot be resolved merely by a multiplicative factor between the observations and suggests a relation of the form

$$(I_{K+F} + I_{A+S})_{HAO} + a = b(I_{K+F} + I_{A+S}). \tag{6}$$

Note that a is the additional sky and instrumental contribution required in the other observations (on the HAO-Pulacayo scale) while b is the scale factor. Parameters a and b appear in Table IV. Although little significance can be attached to the value of a in the K-coronameter data, the positive values in the Waldmeier and Saito results imply a higher sky contribution for these two observations than in the HAO-Pulacayo data. The values of b for the K-coronameter and Saito results appear to be within the limits of accuracy of the data; however, that required by the Waldmeier results appears rather large. In an effort to determine the origin of this discrepancy, Waldmeier, Saito, and Newkirk have initiated a collaborative comparison during the 7 March, 1970 eclipse.

A photometric comparison with the observations of Arnquist and Menzel (1970) is not possible since these authors were not able to place their data on an absolute scale of radiance. Comparison of the isopleths of polarization reveals two differences although the general form of the polarization diagrams are similar. First, these authors measure a maxima of polarization at about 1.5 R in the two streamers in the southern hemisphere of about 45%–50% while our data yield $p_{\max} \sim 35\%$. Second,

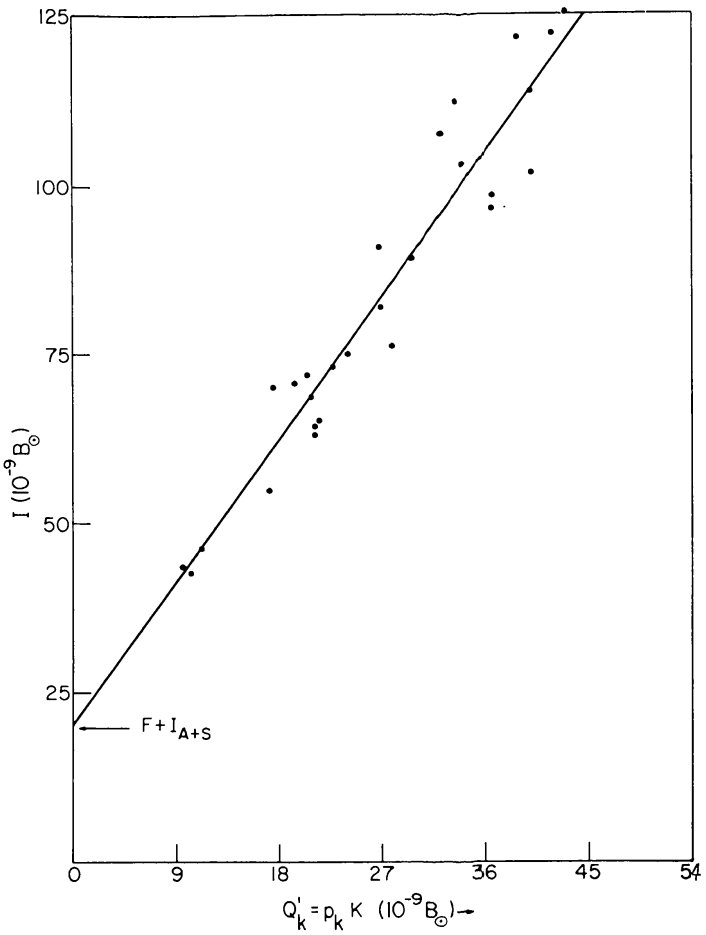

Fig. 8. A sample plot of I vs Q' for latitudes below 50° for $r = 1.67\ R$ used in the separation of the F and K-coronas by the first method.

Arnquist and Menzel find a localized concentration of polarization just east of the north pole which has no counterpart in our observations. At present the origin of these discrepancies is unknown.

TABLE IV

Comparison of observations of the 12 November, 1966 corona

	Waldmeier	Saito	Hansen *et al.* (1967)[a]
a	4.93×10^{-9}	2.95×10^{-9}	1.04×10^{-8}
b	1.95	0.741	1.05

[a] A preliminary evaluation of these intensity scales leads to a complete recalibration of the attenuators used in both the eclipse and K-coronameter observations (Elmore *et al.*, 1970). Table IV makes use of the revised intensity scales.

6. Separation of the F- and K-Coronas

The techniques for separating the contributions of the F- and K-coronas have been extensively discussed in the literature (van de Hulst, 1950; Ney *et al.*, 1961) and need

not be repeated. We here compare the results of two independent methods of separation using the radial scans at latitudes less than 50°.

In the first method we include scans within coronal streamers and assume that:

(1) The polarization of the K-corona is constant at a given radius for all position angles.

(2) The F-corona and sky are unpolarized and functions of radius only.

Thus, the total radiance at a given point is

$$I(\theta) = F + I_{A+S} + p_k^{-1} Q'_k(\theta), \tag{7}$$

and I and Q' for any given radius are linearly related. Here F=radiance of F-corona, p_k=polarization of K-corona, $Q'_k(\theta)=p_k K(\theta)$, and $K(\theta)$=radiance of K-corona.

The accuracy with which Equation (7) represents the data may be judged from Figure 8, which also illustrates the determination of $F+I_{A+S}$. The inferred distribution of the equatorial F-corona as a function of radius appears in Figure 9. It is not surprising that departures from assumption (1) generate uncertainties in the radiance F of from 10 to 30%.

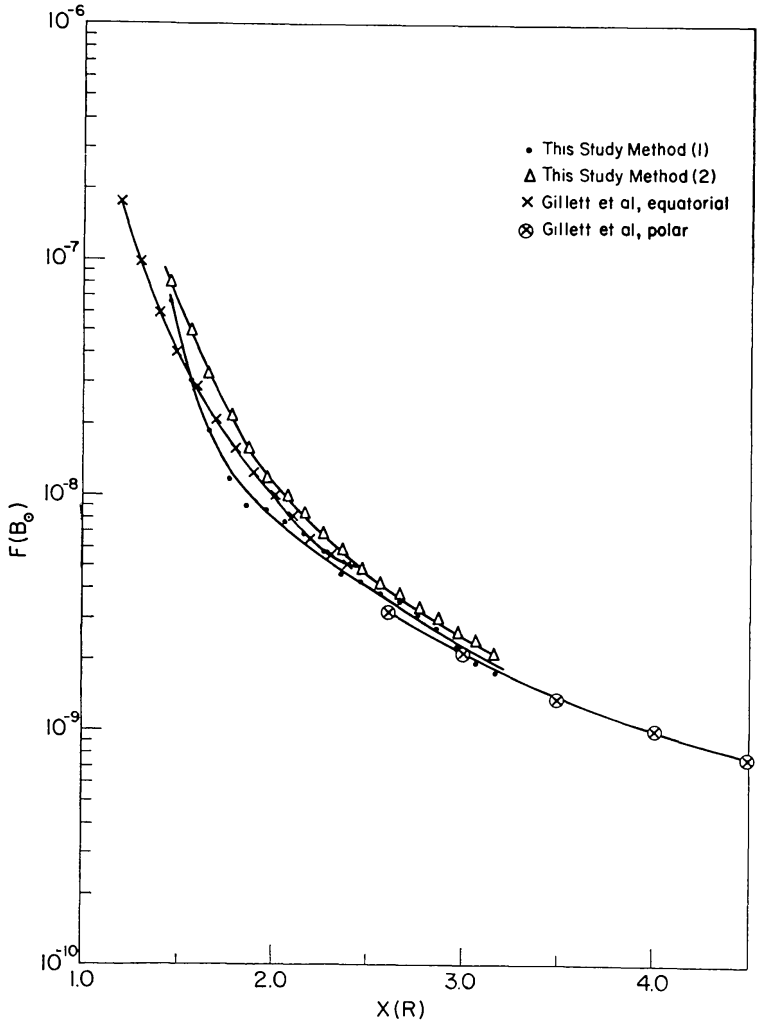

Fig. 9. Radiance of the equatorial F-corona at 6500 Å by the two methods compared to that of Gillett *et al.* (1964) at $\lambda = 4750$ Å.

The second method for separation of the F and K-coronas assumes that an identifiable portion of the corona is azimuthally symmetric. We have chosen this to be the equatorial corona (latitude less than 50°) *excluding* the southeast and southwest streamers. The basic data are I and Q' averaged over position angle in the non-streamer background and both expressed as three term polynomials in X, the projected radius measured in units of R. Again $F+I_{A+S}$ is assumed to be unpolarized, which implies

$$Q'(X) = K_t - K_r = C \int_X^\infty N(r)\{A(r) - B(r)\} \frac{X^2\, dr}{r\sqrt{r^2 - X^2}}, \tag{8}$$

where $N(r)$ is the electron density, $A(r)$ and $B(r)$ are the axes of the vibration ellipsoid for electrons at a distance r for $\lambda = 6500$ Å, and subscripts t and r refer to radiances

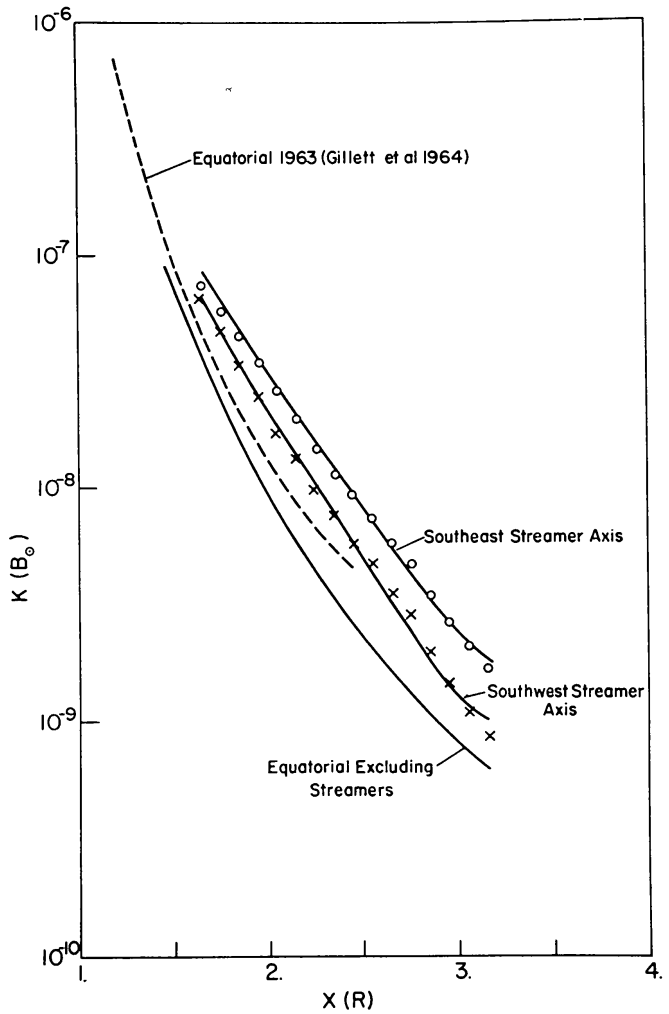

Fig. 10. Radiances of the K-corona in the equatorial zone *excluding* the two major streamers and on the axes of the Southeast and Southwest streamers (○ and ×) compared to the observations of Gillett *et al.* (1964) for 1963 which included all the corona between latitude limits ± 50°. Solid lines for the streamers display the polynomial expressions (12) and (13).

polarized in the tangential and radial directions. To give Q' in units of $10^{-9}\, B_\odot$

$$C = 3.44 \times 10^{-5}\,.$$

Similarly

$$K_t(X) = C \int_X^\infty N(r)\, A(r)\, \frac{r\, dr}{\sqrt{r^2 - X^2}}. \tag{9}$$

For an azimuthally symmetric model, the polynomial expansion for the observed $Q'(X)$ is simply related to that for $N(r)$ and permits an easy determination of the electron densities. Combination of Equations (8) and (9) then yields $K(X) = K_t + K_r$ from which $F(X) + I_{A+S}$ may be determined. The polynomial plotted in Figure 10 corresponds to

$$N(r) = 10^5 (755\, r^{-5.353} - 168\, r^{-14.738} + 103\,800\, r^{-20.446}), \tag{10}$$

which gives the radiance of the F-corona plotted as Method 2 in Figure 9. The photometric results of this separation appear in Table V along with the electron densities for the equatorial zone *excluding* the two streamers.

7. Helmet Streamers

The contributions of the F- and K-coronas inferred from Method 2 in the previous section are assumed to apply equally well to the corona occupied by the two helmet streamers and the resultant quantities K and p_K for the axes of the two major streamers also appear in Table IV and Figure 10. The reduction of these observations for electron density naturally requires more complex assumptions than that for the spherically symmetric component since the line-of-sight extent and the location of the streamer with respect to the plane of the sky are unknown. Use of the polarization to estimate streamer positions and line-of-sight dimensions follows the work of Schmidt (1953), Michard (1954), and Saito *et al.* (1967). We assume the total electron density $N_{(\mathrm{str})}$ in a streamer to be of the form

$$N_{(\mathrm{str})} = N(r) + N_a \exp - \left(\frac{r^2 (\theta - \theta_0)^2}{\tau_1^2} + \frac{r^2 (\phi - \phi_0)^2 \sin^2 \theta}{\tau_2^2} \right), \tag{11}$$

where $N(r)$ is the azimuthally symmetric electron density obtained in the preceding section, and N_a is the enhancement of electron density on the axis of the streamer, expressed as a polynomial in r. The exponent gives the decrease of the enhanced electron density away from the axis of the streamer. Here θ and ϕ are the colatitude and longitude of a point in the streamer, whose axis is at θ_0 and ϕ_0 and τ_1 and τ_2 are the e-folding radii in latitude and longitude, respectively.

For a streamer near the plane of the sky the quantity τ_1 may be deduced directly from the observations (Bohlin, 1968). For ease in computation, we express τ_1 in parametric form. Inspection of Figure 11 suggests that, for the southwest streamer,

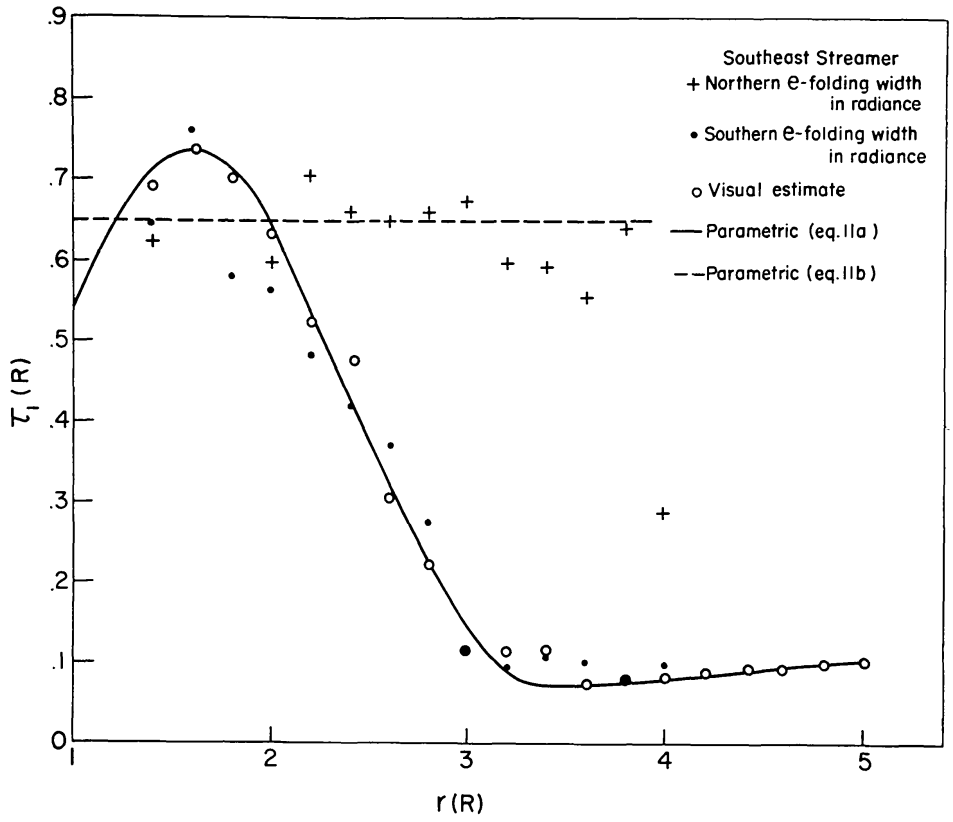

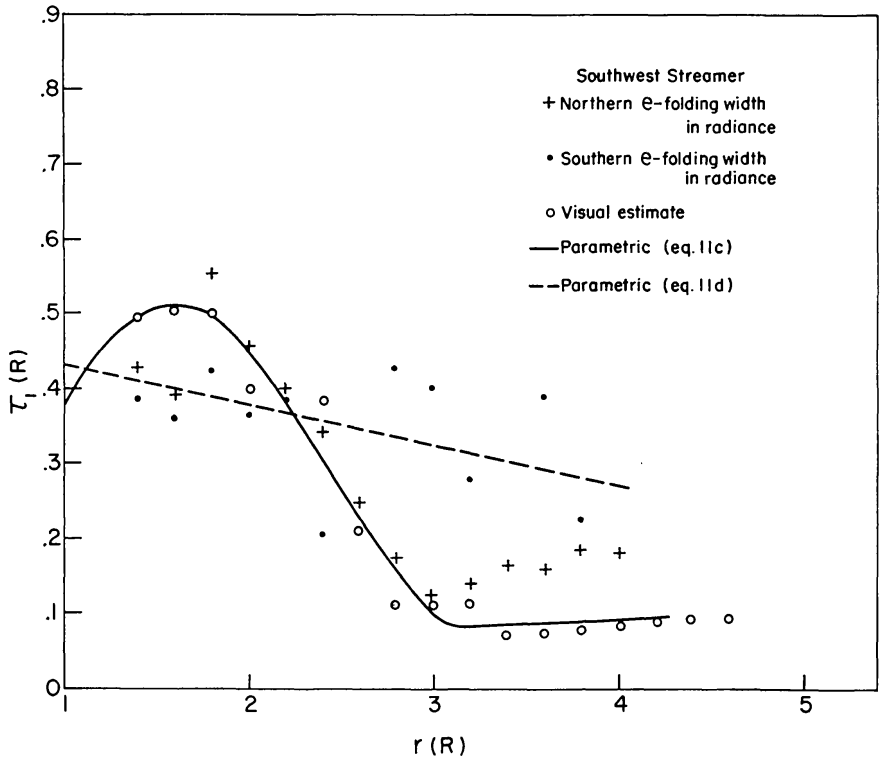

Fig. 11. The *e*-folding radii τ_1 for the two major streamers corrected for the fact that neither streamer was at the limb at the time of the eclipse.

visual estimates of τ_1 from the radially filtered photograph are reliable only for the extension of the streamer to the south of the axis. Here we choose the parametric form

$$\tau_1\,(\text{SE str}) = \begin{cases} 0.739\, e^{-(r-1.6)^2/1.21} & r \leqslant 3.3\,R \\ 0.0018 + 0.02\,r & r \geqslant 3.3\,R \end{cases} \tag{11a}$$

where τ_1 and r are in solar radii. The *northern* extension may be represented by

$$\tau_1\,(\text{SE str}) = 0.65\,. \tag{11b}$$

For the Southwest streamer the *northern* extension is described by

$$\tau_1\,(\text{SW str}) = \begin{cases} 0.505\, e^{-(r-1.6)^2/1.21} & r \leqslant 3.1\,R \\ 0.0167 + 0.02\,r & r \geqslant 3.1\,R \end{cases} \tag{11c}$$

which fits the *southern* extension out to only 2.6 R. A somewhat satisfactory representation of the *southern* extension is

$$\tau_1\,(\text{SW str}) = 0.43 - 0.04\,r\,. \tag{11d}$$

Since, of course, τ_2 the longitudinal extent of the streamer is unknown, we investigate several simple but extreme models of τ_2 for their ability to reproduce the observations of K and p_K along the streamer axes. These are:

(1) An elliptical cross section with

$$\tau_2/\tau_1 = 0.01,\ 0.1,\ 0.25,\ 0.5,\ 1.0,\ 2.0 \text{ or } 3.0$$

and τ_1 given by Equation (11a) or (11c) for their respective streamers;

(2) A radial fan with its plane in the line-of-sight,

$$\tau_2/\tau_1 = \mathrm{d}r,\ \mathrm{d} = 0.087\ (5^\circ),\ 0.174\ (10^\circ),\ 0.261\ (15^\circ).$$

For each of these models equations (8) and (9) were integrated numerically with $N(r)$ replaced by $N(\text{str})$ and with various values of ϕ_0 and the coefficients and powers of N_a in the attempt to reproduce the observed $K(X)$, $Q(X)$, and $p_K(X)$. To evaluate the goodness of fit we determined the squared deviation

$$\sigma^2 = \sum \left(\frac{K_{\text{obs}} - K_{\text{cal}}}{K_{\text{obs}}} \right)^2 + \sum \left(\frac{p_{\text{obs}} - p_{\text{cal}}}{p_{\text{obs}}} \right)^2$$

over the range $1.67\ R \leqslant r \leqslant 2.97\ R$. Table VI demonstrates that *the Southeast streamer appears to be determined rather uniquely as a radial fan with its plane in the line-of-sight and with an e-folding width of* 10° *with* $\phi_0 \sim 140^\circ$ (*or* 220°). The situation with the Southwest streamer is much more ambiguous. *Although* ϕ_0 *is well fixed at* $\sim 20^\circ$ (*or* 340°) *and the form established as an ellipse, any value of* τ_2/τ_1 *from* 0.1 *to* 1.0 *is acceptable!* For the purposes of computing electron densities we choose as final models:

Southeast Streamer

$$N_a = 5180(5000r^{-3.3} + 100r^{-3.2} + 100r^{-7.6})$$
$$\theta_0 = \text{23°S} \quad 113°$$
$$\phi_0 = 140° \text{ (or } 220°) \tag{12}$$
$$\tau_1 \text{ (see Equations (11a) and (11b))}$$
$$\tau_2 = 10° \text{ in longitude}$$

Southwest Streamer

$$N_a = 606(5000r^{-1.9} + 100r^{-3.2} + 100r^{-7.6})$$
$$\theta_0 = \text{28°S} \quad 118°$$
$$\phi_0 = 20° \text{ (or } 340°) \tag{13}$$
$$\tau_1 \text{ (see Equations (11c) and (11d))}$$
$$\tau_2 = \tau_1$$

The calculated variations of K on a radius along each of the streamer axes are compared to the observations in Figure 10 while the corresponding comparisons of ob-

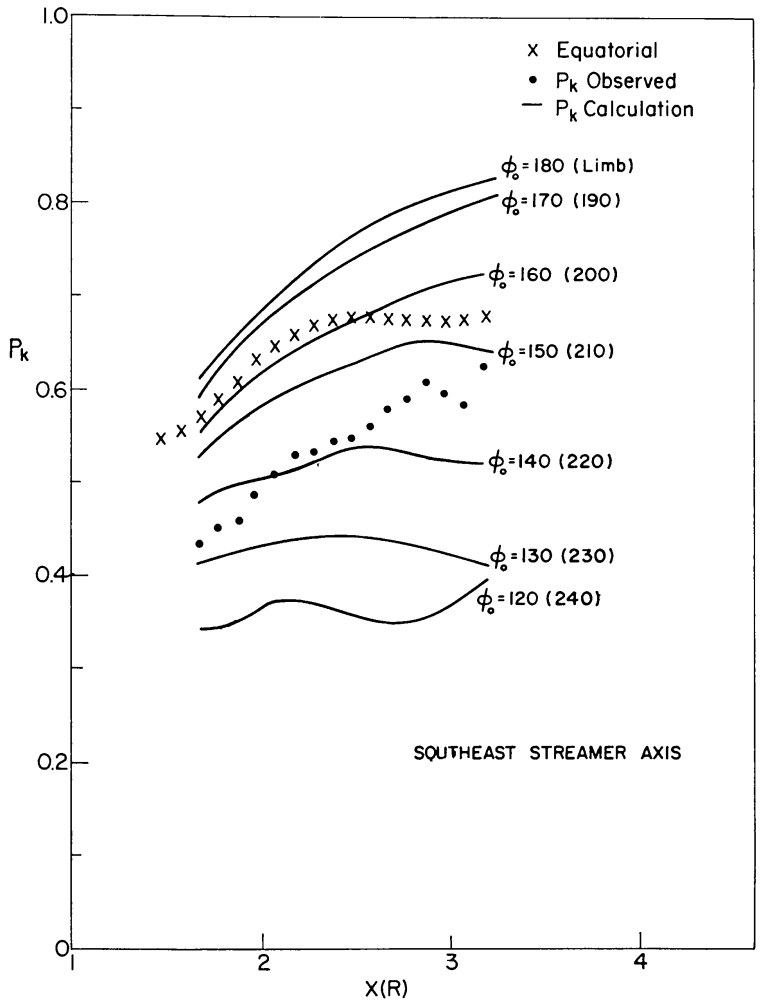

Fig. 12a.

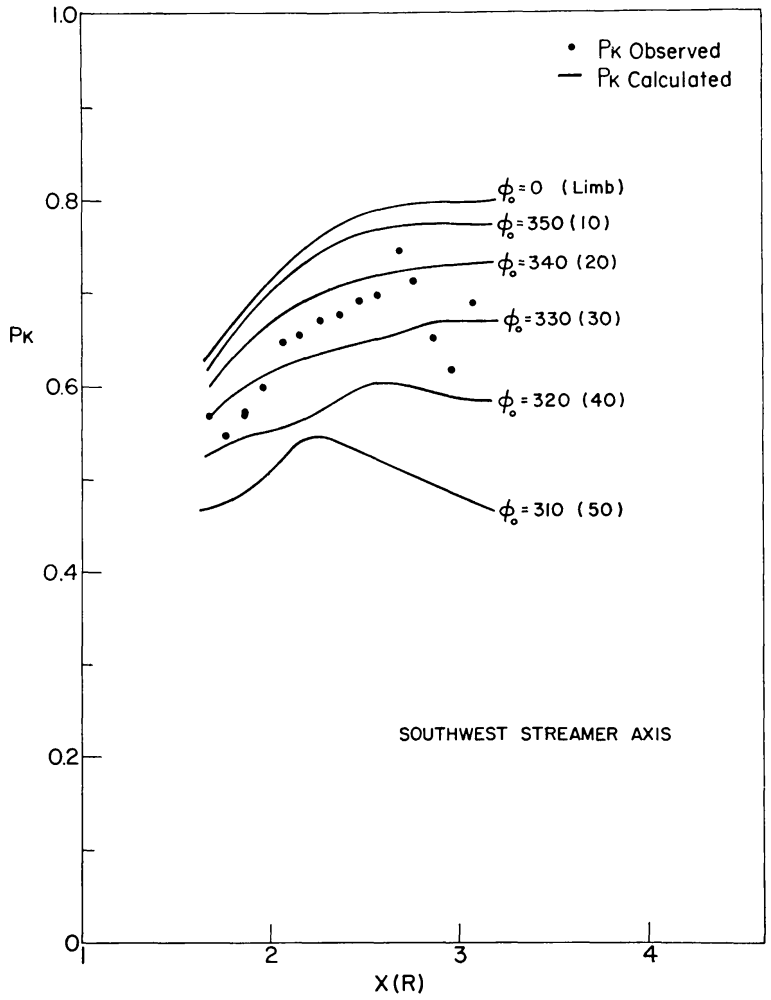

Fig. 12b.

Figs. 12a and b. Variation of p_K along the axes of the two major streamers as observed and as calculated for the models. The variation of p_K for the equatorial zone excluding streamers appears for comparison only.

served and calculated $p_K(X)$ appear in Figures 12a and b. Table V contains the inferred axial electron densities for the two streamers.

Although the parameters finally chosen to represent the two streamers give reasonably good fits to the observations, the final models have little claim to uniqueness. We have not attempted to make a least-squares determination for any of the parameters. Several comments are in order regarding the influence of the different quantities on the results. First, θ_0 is not an independent parameter since it is determined by ϕ_0 and the observed position angle. Second, the form of $K(X)$ is largely determined by the forms of $N(\text{str})$ and $\tau_2(r)$ with ϕ_0 having little direct influence. On the other hand, $p_K(X)$ is strongly influenced by the parameters ϕ_0 and τ_2, which determine the distribution of electrons with respect to the plane of the sky. We have made use of these facts in the iterations employed to arrive at the final parameters. For any given model of τ_2 the electron densities N_a may be roughly set to bring about agreement with $K(X)$ independently of ϕ_0. Comparison of the observed and calculated p_K gives a

TABLE V

Radius	Azimuthally symmetric 'equatorial' background					Axis of SE streamer				Axis of SW streamer			
	F[a]	K[a]	N_e[b]	T_e[c]	p_k	K[a]	N_e[b]	T_e[c]	p_k	K[a]	N_e[b]	T_e[c]	p_k
1.67	32.15	35.29	5.34		0.57	76.37	10.01		0.44	62.69	6.29		0.59
1.77	21.64	23.19	3.71	1.37	0.59	57.89	7.66	1.76	0.45	45.88	4.67	1.58	0.56
1.87	15.82	15.74	2.68	1.38	0.61	46.30	6.03	1.77	0.46	33.44	3.61	1.63	0.57
1.97	11.38	11.00	1.99	1.35	0.63	34.52	4.84	1.73	0.49	23.95	2.86	1.63	0.61
2.07	9.81	7.89	1.51	1.30	0.64	25.92	3.94	1.68	0.51	17.35	2.31	1.61	0.65
2.17	8.00	5.80	1.16	1.24	0.66	19.80	3.25	1.63	0.53	13.08	1.90	1.59	0.66
2.27	6.71	4.35	0.91	1.19	0.66	14.95	2.71	1.57	0.53	9.81	1.58	1.57	0.67
2.37	5.69	3.33	0.73	1.14	0.67	11.27	2.28	1.52	0.54	7.40	1.34	1.55	0.68
2.47	4.88	2.59	0.59	1.09	0.67	9.28	1.94	1.47	0.55	5.65	1.14	1.54	0.70
2.57	4.12	2.04	0.48	1.05	0.67	7.31	1.66	1.43	0.56	4.58	0.99	1.52	0.71
2.67	3.68	1.63	0.39	1.01	0.67	5.69	1.43	1.39	0.58	3.42	0.86	1.51	0.77
2.77	3.23	1.32	0.32	0.97	0.67	4.65	1.24	1.35	0.59	2.69	0.76	1.51	0.76
2.87	2.91	1.08	0.27	0.93	0.67	3.41	1.08	1.31	0.61	1.86	0.68	1.50	0.69
2.97	2.59	0.89	0.23	0.90	0.67	2.63	0.95	1.27	0.60	1.34	0.61	1.49	0.66
3.07	2.32	0.74	0.19	0.87	0.68	2.07	0.84	1.24	0.58	0.97	0.55	1.48	0.77
3.17	2.08	0.62	0.17	0.84	0.68	1.69	0.75	1.21	0.63	0.74	0.50	1.48	0.89

[a] Unit $10^{-9}\ B_\odot$
[b] Unit 10^6 cm^{-3}
[c] Unit 10^6 K

TABLE VI

The squared deviation σ^2 for various models

		Elliptical $-\tau_2/\tau_1$							Radial fan		
	ϕ_0	0.01	0.1	0.25	0.5	1.0	2.0	3.0	5°	10°	15°
Southwest streamer	120 (240)	5.075	5.291	5.333	5.769	9.171	4.861	4.670	2.679	2.163	2.386
	130 (230)	3.259	3.821	2.984	3.455	3.884	3.892	3.707	1.094	0.873	1.040
	140 (220)	2.087	2.961	2.840	2.983	3.168	3.108	2.898	0.439	*0.131*	0.258
	150 (210)	1.999	2.598	2.626	2.696	2.778	2.631	2.378	1.140	0.667	0.680
	160 (200)	2.936	2.933	2.938	2.938	2.861	2.542	2.245	2.664	2.189	1.972
	170 (190)	4.153	3.654	3.623	3.523	3.244	2.712	2.339	4.087	3.730	3.271
	180 (limb)	5.262	4.063	3.988	3.831	3.447	2.810	2.399	4.666	4.330	3.831
Southwest streamer	310 (50)	2.512	2.493	2.394	2.096	1.588	1.232	1.071	1.194	1.242	1.369
	320 (40)	0.786	0.776	0.771	0.752	0.689	0.544	0.488	0.518	0.541	0.622
	330 (30)	0.298	0.255	0.252	0.241	0.211	0.168	0.171	0.162	0.124	0.163
	340 (20)	0.249	0.101	0.102	*0.104*	0.117	0.195	0.355	0.186	0.125	0.124
	350 (10)	1.980	0.275	0.276	0.282	0.307	0.455	0.729	0.374	0.305	0.251
	0 (limb)	0.405	0.368	0.387	0.394	0.418	0.583	0.898	0.472	0.409	0.313

first estimate of ϕ_0 which is then used to improve the model of N_a for any particular model of τ_2.

Fortunately, the ambiguity inherent in the determination of ϕ_0 could be removed by reference to other data. In Figures 13a and b we compare the inferred positions of the two streamers with isopleths of Q' made by the High Altitude Observatory K-coronameter at Mauna Loa, Hawaii and kindly supplied us by R. T. Hansen. The central meridians of a and b coincide, respectively, with the east and west limbs at the time of eclipse and the alternate positions of the two streamers appear. Although the inferred position of the southeast streamer is somewhat east of the center of gravity of the feature β' in the K-coronameter, our choice of $\phi_0 = 140°$ over $\phi_0 = 220°$ appears justified. Similarly, the identification of the southwest streamer with feature δ and the choice of $\phi_0 = 20°$ is without serious question. Thus, we conclude that these two major streamers were significantly behind the solar limb at the time of eclipse in agreement with the conclusion of Hansen *et al.* (1967) based solely on K-coronameter observations.

8. Electron Densities and Temperatures

Electron densities for the equatorial zone and for the axes of the two helmet streamers are compared with similar data from other eclipses in Figure 14. We see immediately that our equatorial densities are only somewhat above those of the van de Hulst (1950) minimum equatorial corona. This rather surprising fact is apparently due to our exclusion of the streamers from this analysis. The comparison of our streamer densities with other models serves to demonstrate both that there is a great deal of variation from one streamer to the next and that the assumptions regarding the line of sight extent of the streamer have rather profound effect on the model. This point is illustrated by the Michard (1954) and Hepburn (1955) results for the same streamers. One common characteristic of these helmet streamers is apparent, however; all show an enhancement above the background (here taken as the equatorial zone) which increases from 1.2 or more at $\sim 1.5\ R$ to 3 to 20 at $\sim 3\ R$. Again, the exact value and dependence upon r of this augmentation appears to vary considerably from feature to

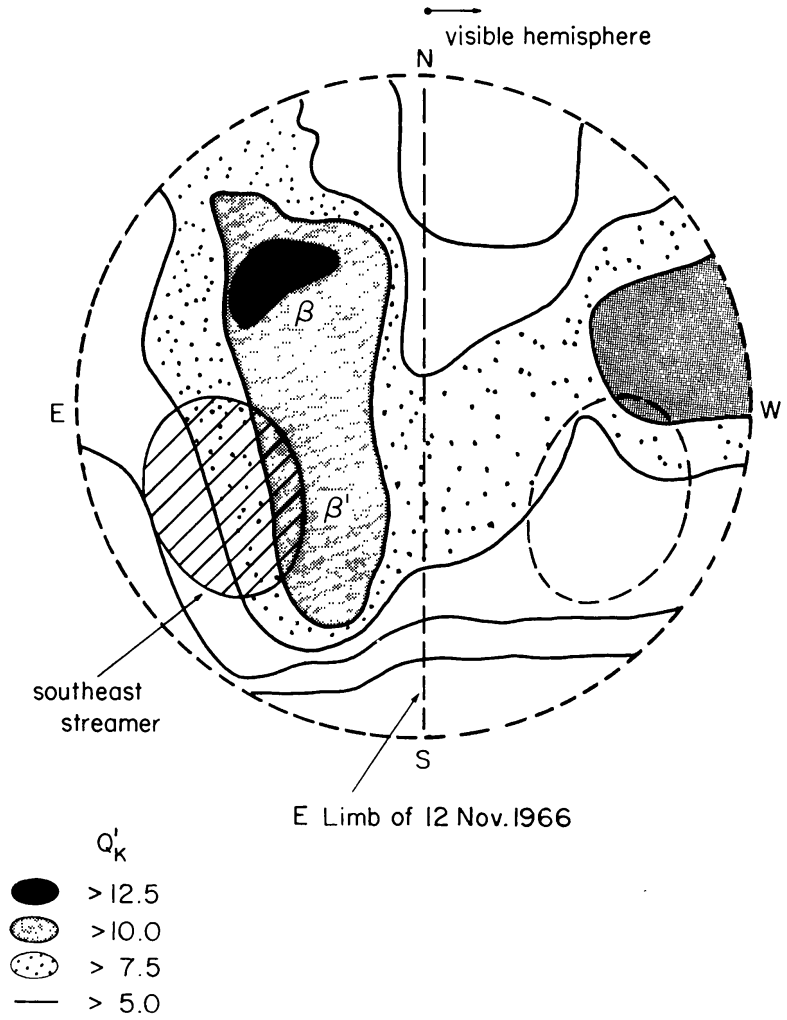

Fig. 13a.

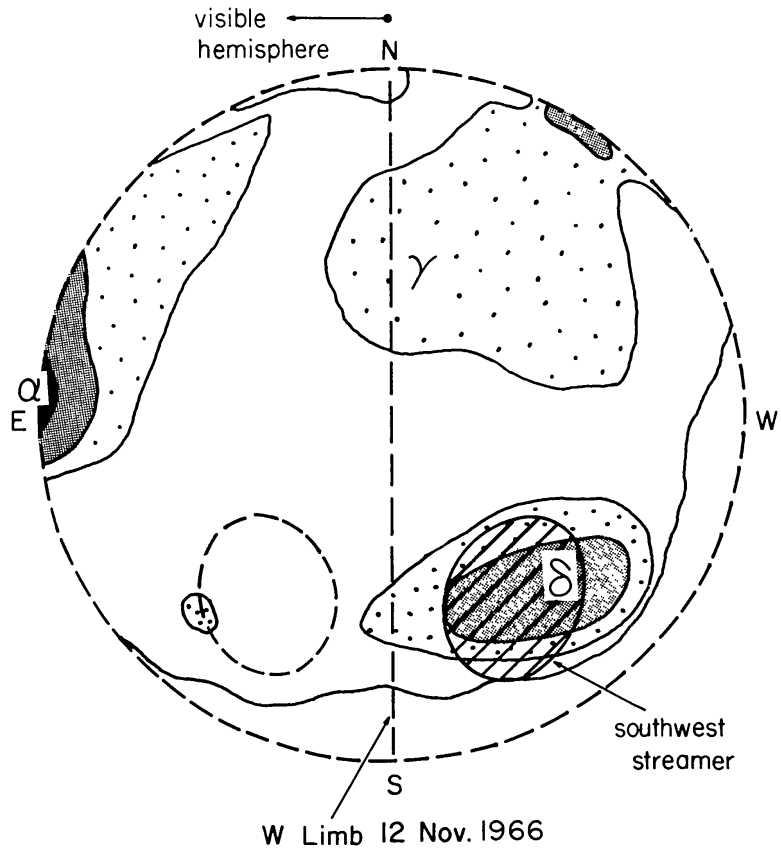

Fig. 13b.

Figs. 13a and b. Isopleths of Q'_K measured by the K-coronameter at 1.5 R during November 1966. The east and west limbs at the time of eclipse correspond to the central meridians of a and b, respectively. The alternate position of the two streamers inferred from the polarization analysis are indicated by ellipses.

feature although this fact also reflects the different assumptions concerning streamer geometry used in the reduction.

For a corona in steady state expansion, the temperature is related to the density by (Billings, 1966)

$$\frac{1}{T_e}\frac{dT_e}{dr} = -\frac{1}{N}\frac{dN}{dr} - \frac{\mu m_H}{kT_e}\left(\frac{g}{r^2} + \frac{v}{R}\frac{dv}{dr}\right), \tag{14a}$$

where we take $\mu = 0.608 =$ mean molecular weight for a hydrogen to helium ratio of 10 to 1, $m_H =$ mass of hydrogen atom, $g =$ surface gravity, $r =$ radius in units of R, $v =$ expansion velocity. If the change in temperature between two levels is negligible, then for a static corona

$$\frac{d\ln N}{d(1/r)} = \frac{\mu g m_H R}{k}\frac{1}{T_e}, \tag{14b}$$

which we use to estimate temperatures in the equatorial zone and on the axes of the two streamers with the result shown in Figure 15. Two conclusions are immediately apparent. First, although little significance can be placed upon the differences between

our models and those for other streamers observed at different parts of the solar cycle, the elevated temperature in a streamer compared to the equatorial background appears well established. Second, the critical role of the geometrical assumptions made in reducing the observations is emphasized by the disparate temperature profiles derived for the Southwest streamer with various values of τ_2/τ_1. One suspects that some of these models may be physically unrealistic although this cannot be demonstrated from

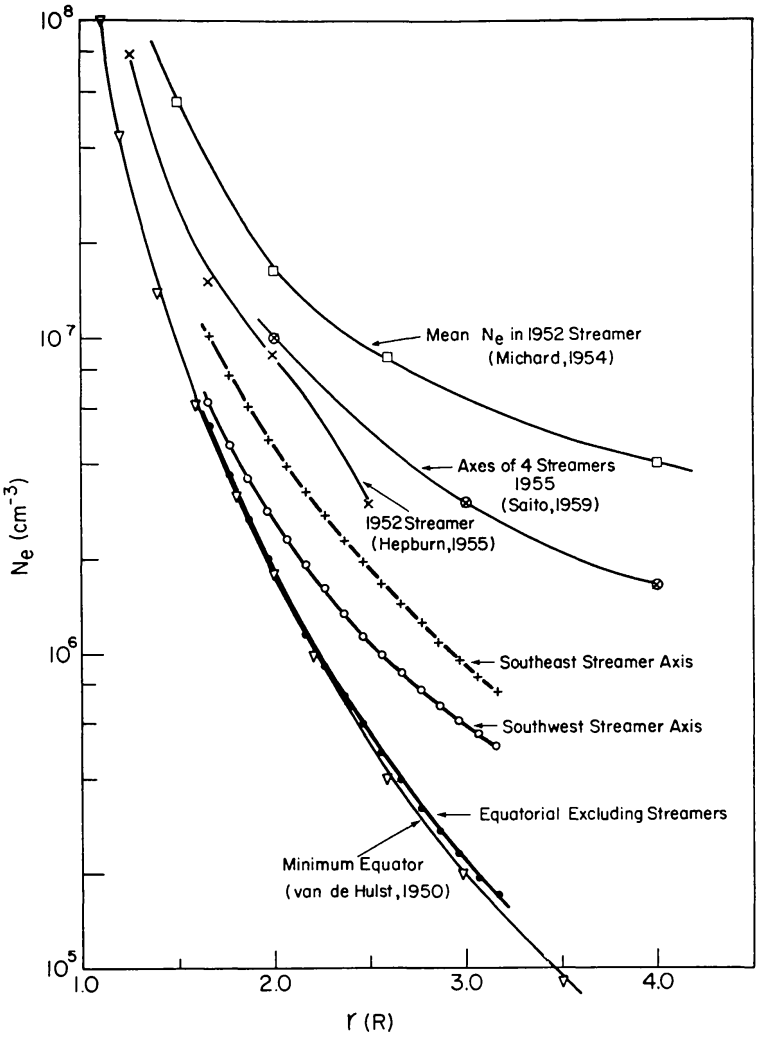

Fig. 14. Electron densities for the two streamers and for the equatorial zone excluding the streamers compared with those derived from other eclipses.

the observations alone. Of course, any statements regarding coronal streamer temperatures from equation (14b) must be made with full awareness that below $\sim 2\ R$ the influence of magnetic fields must be included and that above $\sim 3\ R$ the dynamical terms in (14a) must be considered. An evaluation of the density and temperature structure of these two streamers in terms of a dynamical model (Pneuman and Kopp, 1970) relating the density, temperatures, and magnetic fields at their bases is to be considered in a subsequent paper.

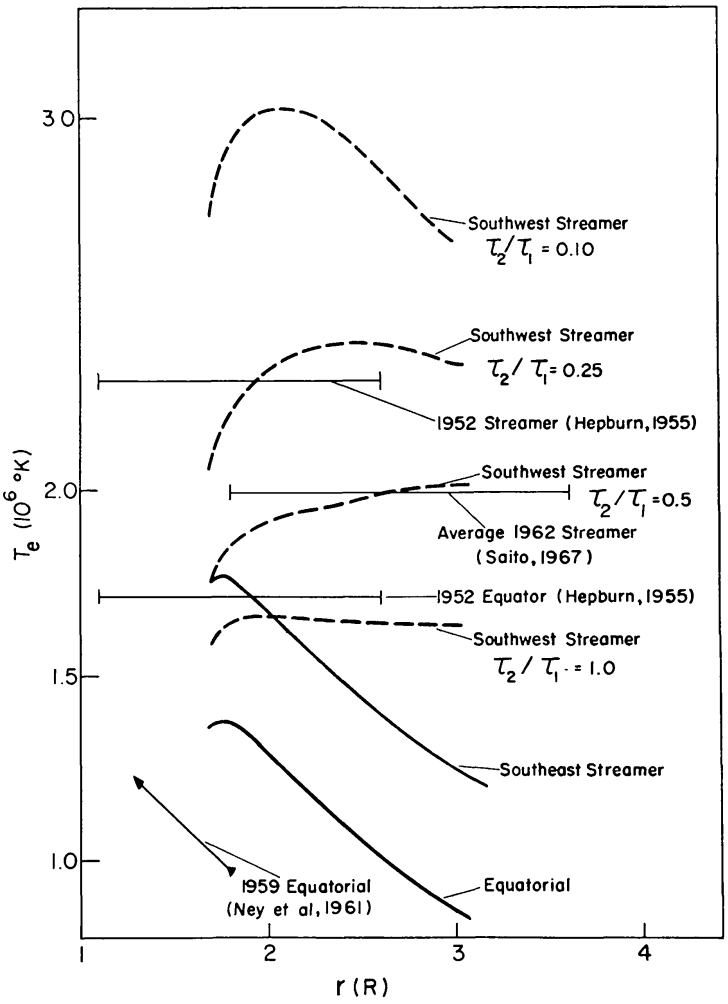

Fig. 15. Electron temperatures derived from the assumption of hydrostatic equilibrium for the equatorial zone and for the axes of several streamers. Note that the Ney *et al.* data averaged all the corona between latitude limits $\pm 50°$ while the present study excludes the streamers.

Acknowledgements

The observations for this analysis could not have been made without the enthusiastic support of Dr. H. S. Ahluwalia and his staff at the Laboratorio Física Cósmica, La Paz, Bolivia. Technical development of the equipment was under the supervision of L. Lacey and H. Hull, both of whom assisted in making the observations. D. King and C. Smythe aided in their reduction.

References

Arnquist, W. N. and Menzel, D. H.: 1970, *Solar Phys.* **11**, 82.
Billings, D. E.: 1966, *A Guide to the Solar Corona*, Academic Press, New York, p. 251.
Blackwell, D. E. and Petford, A. D.: 1966, *Monthly Notices Roy. Astron. Soc.* **131**, 383.
Bohlin, J. D.: 1968, Ph.D. Thesis, University of Colorado, Dept. of Astro-Geophysics.
Elmore, D. F., Streete, J. L., and Eddy, J. A.: 1970, 'Calibration of Opal Glass Attenuators', Astro-Geophysical Memorandum No. 178.
Gillett, F. C., Stein, W. A., and Ney, E. P.: 1964, *Astrophys. J.* **140**, 292.

Hansen, R., Hansen, S., and Garcia, C.: 1967, 'The Solar Electron Corona of 12 November, 1966', Astro-Geophysical Memorandum No. 174.
Hata, S. and Saito, K.: 1966, *Ann. Tokyo Astron. Observ.*, 2nd Ser. **10**, 16.
Hepburn, N.: 1955, *Astrophys. J.* **122**, 445.
Michard, R.: 1954, *Ann. Astrophys.* **17**, 429.
Ney, E. P., Huch, W. F., Kellogg, P. J., Stein, W., and Gillett, F.: 1961, *Astrophys. J.* **133**, 616.
Pneuman, G. and Kopp, R.: 1970, *Solar Phys.* **13**, 176.
Saito, K.: 1959, *Publ. Astron. Soc. Japan* **11**, 234.
Saito, K. and Owaki, N.: 1967, *Publ. Astron. Soc. Japan* **19**, 535.
Schmidt, M.: 1953, *Bull. Astron. Inst. Neth.* **12**, 61.
Shurcliff, W. A.: 1962, *Polarized Light*, Harvard Univ. Press, Cambridge, Mass.
Van de Hulst, H. C.: 1950, *Bull. Astron. Inst. Neth.* **11**, 135.
Waldmeier, M.: 1967, *Z. Astrophys.* **67**, 463.